

# A sub-100fs self-starting Cr:forsterite laser generating 1.4W output power

Shih-Hsuan Chia,<sup>1</sup> Tzu-Ming Liu,<sup>2,6</sup> Anatoly A. Ivanov,<sup>3</sup> Andrey B. Fedotov,<sup>4</sup>  
Aleksey M. Zheltikov,<sup>4</sup> Ming-Rung Tsai,<sup>1</sup> Ming-Che Chan,<sup>1</sup> Che-Hang Yu,<sup>1</sup>  
and Chi-Kuang Sun<sup>1,5\*</sup>

<sup>1</sup>Graduate Inst. of Photonics and Optoelectronics and Department of Electrical Engineering, Natl. Taiwan Univ., Taipei 10617, Taiwan

<sup>2</sup>Inst. of Biomedical Engineering, Natl. Taiwan Univ., Taipei 10617, Taiwan

<sup>3</sup>Photochemistry Cent., Russian Acad. of Sciences, ul. Novatorov 7a, Moscow 117421, Russia

<sup>4</sup>Moscow MV Lomonosov State Univ, Dept. Phys. Ctr. Int. Laser, Moscow 119992, Russia

<sup>5</sup>Research Center for Applied Sciences, Academia Sinica, Taipei 115, Taiwan

<sup>6</sup>tmlu@ntu.edu.tw

\*sun@cc.ee.ntu.edu.tw

**Abstract:** Without cavity dumping or external amplification, we report a femtosecond Cr:forsterite laser with a 1.4W output power and 2W in continuous wave (CW) operated with a crystal temperature of 267K. In the femtosecond regime, the oscillator generates Kerr-lens-mode-locked 84fs pulses with a repetition rate of 85MHz, corresponding to a high 16.5nJ pulse energy directly from a single Cr:forsterite resonator. This intense femtosecond Cr:forsterite laser is ideal to pump varieties of high power fiber light sources and could be thus ideal for many biological and spectroscopy applications.

©2010 Optical Society of America

OCIS codes: (320.7090) Ultrafast lasers; (140.3580) Lasers, solid-state.

---

## References and links

1. T. J. Carrig, and C. R. Pollock, "Tunable, cw operation of a multiwatt forsterite laser," *Opt. Lett.* **16**(21), 1662–1664 (1991).
2. B. E. Bouma, G. J. Tearney, I. P. Bilinsky, B. Golubovic, and J. G. Fujimoto, "Self-phase-modulated Kerr-lens mode-locked Cr:forsterite laser source for optical coherence tomography," *Opt. Lett.* **21**(22), 1839–1841 (1996).
3. G. J. Tearney, B. E. Bouma, S. A. Boppart, B. Golubovic, E. A. Swanson, and J. G. Fujimoto, "Rapid acquisition of *in vivo* biological images by use of optical coherence tomography," *Opt. Lett.* **21**(17), 1408–1410 (1996).
4. C.-K. Sun, S.-W. Chu, S.-Y. Chen, T.-H. Tsai, T.-M. Liu, C.-Y. Lin, and H.-J. Tsai, "Higher harmonic generation microscopy for developmental biology," *J. Struct. Biol.* **147**(1), 19–30 (2004).
5. C.-S. Hsieh, S.-U. Chen, Y.-W. Lee, Y.-S. Yang, and C.-K. Sun, "Higher harmonic generation microscopy of *in vitro* cultured mammal oocytes and embryos," *Opt. Express* **16**(15), 11574–11588 (2008).
6. I.-H. Chen, S.-W. Chu, C.-K. Sun, P. C. Cheng, and B.-L. Lin, "Wavelength dependent damage in biological multi-photon confocal microscopy: A micro-spectroscopic comparison between femtosecond Ti:sapphire and Cr:forsterite laser sources," *Opt. Quantum Electron.* **34**(12), 1251–1266 (2002).
7. S.-Y. Chen, S.-U. Chen, H.-Y. Wu, W.-J. Lee, Y.-H. Liao, and C.-K. Sun, "In Vivo Virtual Biopsy of Human Skin by Using Noninvasive Higher Harmonic Generation Microscopy," *IEEE J. Sel. Top. Quantum Electron.* **16**(3), 478–492 (2010).
8. S.-W. Chu, I.-H. Chen, T.-M. Liu, P. C. Chen, C.-K. Sun, and B.-L. Lin, "Multimodal nonlinear spectral microscopy based on a femtosecond Cr:forsterite laser," *Opt. Lett.* **26**(23), 1909–1911 (2001).
9. T.-M. Liu, S.-W. Chu, C.-K. Sun, B.-L. Lin, P. C. Cheng, and I. Johnson, "Multiphoton confocal microscopy using a femtosecond Cr:forsterite laser," *Scanning* **23**(4), 249–254 (2001).
10. T.-H. Tsai, C.-Y. Lin, H. J. Tsai, S. Y. Chen, S. P. Tai, K. H. Lin, and C.-K. Sun, "Biomolecular imaging based on far-red fluorescent protein with a high two-photon excitation action cross section," *Opt. Lett.* **31**(7), 930–932 (2006).
11. S.-Y. Chen, H.-Y. Wu, and C.-K. Sun, "*In vivo* harmonic generation biopsy of human skin," *J. Biomed. Opt.* **14**(6), 060505 (2009).
12. J.-H. Lee, S.-Y. Chen, C.-H. Yu, S.-W. Chu, L.-F. Wang, C. K. Sun, and B. L. Chiang, "Noninvasive *in vitro* and *in vivo* assessment of epidermal hyperkeratosis and dermal fibrosis in atopic dermatitis," *J. Biomed. Opt.* **14**(1), 014008 (2009).
13. C.-K. Sun, C.-C. Chen, S.-W. Chu, T.-H. Tsai, Y.-C. Chen, and B.-L. Lin, "Multiharmonic-generation biopsy of skin," *Opt. Lett.* **28**(24), 2488–2490 (2003).

14. S.-P. Tai, W.-J. Lee, D.-B. Shieh, P.-C. Wu, H.-Y. Huang, C.-H. Yu, and C.-K. Sun, "In vivo optical biopsy of hamster oral cavity with epi-third-harmonic-generation microscopy," *Opt. Express* **14**(13), 6178–6187 (2006).
15. S.-P. Tai, Y. Wu, D.-B. Shieh, L.-J. Chen, K.-J. Lin, C.-H. Yu, S.-W. Chu, C.-H. Chang, X.-Y. Shi, Y.-C. Wen, K.-H. Lin, T.-M. Liu, and C.-K. Sun, "Molecular imaging of cancer cells using plasmon-resonant-enhanced third-harmonic-generation in silver nanoparticles," *Adv. Mater.* **19**(24), 4520–4523 (2007).
16. C.-H. Yu, S.-P. Tai, C.-T. Kung, W.-J. Lee, Y.-F. Chan, H.-L. Liu, J.-Y. Lyu, and C.-K. Sun, "Molecular third-harmonic-generation microscopy through resonance enhancement with absorbing dye," *Opt. Lett.* **33**(4), 387–389 (2008).
17. S.-H. Chia, C.-H. Yu, C.-H. Lin, N.-C. Cheng, T.-M. Liu, M.-C. Chan, I.-H. Chen, and C.-K. Sun, "Miniaturized video-rate epi-third-harmonic-generation fiber-microscope," *Opt. Express* **18**(16), 17382–17391 (2010).
18. W.-J. Lee, C. F. Lee, S. Y. Chen, Y.-S. Chen, and C.-K. Sun, "Virtual biopsy of rat tympanic membrane using higher harmonic generation microscopy," *J. Biomed. Opt.* **15**(4), 046012 (2010).
19. S.-P. Tai, T.-H. Tsai, W.-J. Lee, D.-B. Shieh, Y.-H. Liao, H.-Y. Huang, K. Y.-J. Zhang, H.-L. Liu, and C.-K. Sun, "Optical biopsy of fixed human skin with backward-collected optical harmonics signals," *Opt. Express* **13**(20), 8231–8242 (2005).
20. S.-W. Chu, S.-Y. Chen, G.-W. Chern, T.-H. Tsai, Y.-C. Chen, B.-L. Lin, and C.-K. Sun, "Studies of  $\chi^{(2)}/\chi^{(3)}$  tensors in submicron-scaled bio-tissues by polarization harmonics optical microscopy," *Biophys. J.* **86**(6), 3914–3922 (2004).
21. R. R. Anderson, W. Farinelli, H. Laubach, D. Manstein, A. N. Yaroslavsky, J. Gubeli 3rd, K. Jordan, G. R. Neil, M. Shinn, W. Chandler, G. P. Williams, S. V. Benson, D. R. Douglas, and H. F. Dylla, "Selective photothermolysis of lipid-rich tissues: a free electron laser study," *Lasers Surg. Med.* **38**(10), 913–919 (2006).
22. K. Suto, T. Sasaki, T. Tanabe, K. Saito, J.-I. Nishizawa, and M. Ito, "GaP THz wave generator and THz spectrometer using Cr:forsterite lasers," *Rev. Sci. Instrum.* **76**(12), 123109 (2005).
23. T. Dennis, E. A. Curtis, C. W. Oates, L. Hollberg, and S. L. Gilbert, "Wavelength References for 1300-nm Wavelength-Division Multiplexing," *J. Lightwave Technol.* **20**(5), 776–782 (2002).
24. M.-C. Chan, T.-M. Liu, S.-P. Tai, and C.-K. Sun, "Compact fiber-delivered Cr:forsterite laser for nonlinear light microscopy," *J. Biomed. Opt.* **10**(5), 054006 (2005).
25. M.-C. Chan, S.-W. Chu, C.-H. Tseng, Y.-C. Wen, Y.-H. Chen, G.-D. J. Su, and C.-K. Sun, "Cr:Forsterite-laser-based fiber-optic nonlinear endoscope with higher efficiencies," *Microsc. Res. Tech.* **71**(8), 559–563 (2008).
26. A. V. Mitrofanov, A. A. Ivanov, M. V. Alfimov, A. A. Podshivalov, and A. M. Zheltikov, "Microjoule supercontinuum generation by stretched megawatt femtosecond laser pulses in a large-mode-area photonic-crystal fiber," *Opt. Commun.* **280**, 453–456 (2007).
27. A. B. Fedotov, D. A. Sidorov-Biryukov, A. A. Ivanov, M. V. Alfimov, V. I. Beloglazov, N. B. Skibina, C.-K. Sun, and A. M. Zheltikov, "Soft-glass photonic-crystal fibers for frequency shifting and white-light spectral superbroadening of femtosecond Cr:forsterite laser pulses," *J. Opt. Soc. Am. B* **23**(7), 1471–1477 (2006).
28. M.-C. Chan, S.-H. Chia, T.-M. Liu, T.-H. Tsai, M.-C. Ho, A. A. Ivanov, A. M. Zheltikov, J.-Y. Liu, H.-L. Liu, and C.-K. Sun, "1.2–2.2- $\mu\text{m}$  tunable Raman soliton source based on a Cr:forsterite-laser and a photonic-crystal fiber," *IEEE Photon. Technol. Lett.* **20**(11), 900–902 (2008).
29. M.-C. Chan, P.-C. Peng, Y. Lai, S. Chi, and C.-K. Sun, "Continuously-Tunable Large-Dynamic-Range RF Phase Shifter via a Soliton Self-Frequency-Shifted Source and a Dispersive Fiber," *IEEE Photon. Technol. Lett.* **21**(5), 313–315 (2009).
30. V. Petričević, S. K. Gayen, R. R. Alfano, K. Yamagishi, H. Anzai, and Y. Yamaguchi, "Laser action in chromium-doped forsterite," *Appl. Phys. Lett.* **52**(13), 1040–1042 (1988).
31. T. J. Carrig, and C. R. Pollock, "Performance of a Continuous-Wave Forsterite Laser with Krypton Ion, Ti:Sapphire and Nd:YAG Pump Lasers," *IEEE J. Quantum Electron.* **29**(11), 2835–2844 (1993).
32. N. Zhavoronkov, A. Avtikh, and V. Mikhailov, "Chromium-doped forsterite laser with 1.1 W of continuous-wave output power at room temperature," *Appl. Opt.* **36**(33), 8601–8605 (1997).
33. V. Yanovsky, Y. Pang, F. Wise, and B. I. Minkov, "Generation of 25-fs pulses from a self-mode-locked Cr:forsterite laser with optimized group-delay dispersion," *Opt. Lett.* **18**(18), 1541–1543 (1993).
34. C. Chudoba, J. G. Fujimoto, E. P. Ippen, H. A. Haus, U. Morgner, F. X. Kärtner, V. Scheuer, G. Angelow, and T. Tschudi, "All-solid-state Cr:forsterite laser generating 14-fs pulses at 1.3  $\mu\text{m}$ ," *Opt. Lett.* **26**(5), 292–294 (2001).
35. A. A. Ivanov, B. I. Minkov, G. Jonusauskas, J. Oberlé, and C. Rullière, "Influence of  $\text{Cr}^{4+}$  ion concentration on cw operation of forsterite laser and its relation to thermal problems," *Opt. Commun.* **116**(1-3), 131–135 (1995).
36. A. Sennaroglu, "Analysis and optimization of lifetime thermal loading in continuous-wave  $\text{Cr}^{4+}$ -doped solid-state lasers," *J. Opt. Soc. Am. B* **18**(11), 1578–1586 (2001).
37. N. V. Kuleshov, A. V. Podlipensky, V. G. Shcherbitsky, A. A. Lagatsky, and V. P. Mikhailov, "Excited-state absorption in the range of pumping and laser efficiency of  $\text{Cr}^{4+}$ :forsterite," *Opt. Lett.* **23**(13), 1028–1030 (1998).
38. E. Slobodchikov, J. Ma, V. Kamalov, K. Tominaga, and K. Yoshihara, "Cavity-dumped femtosecond Kerr-lens mode locking in a chromium-doped forsterite laser," *Opt. Lett.* **21**(5), 354–356 (1996).
39. G. Jonusauskas, J. G. Oberlé, and C. Rullière, "54-fs, 1-GW, 1-kHz pulse amplification in Cr:forsterite," *Opt. Lett.* **23**(24), 1918–1920 (1998).
40. V. Shcheslavskiy, V. V. Yakovlev, and A. Ivanov, "High-energy self-starting femtosecond  $\text{Cr}^{4+}$ : $\text{Mg}_2\text{SiO}_4$  oscillator operating at a low repetition rate," *Opt. Lett.* **26**(24), 1999–2001 (2001).
41. H. Cankaya, J. G. Fujimoto, and A. Sennaroglu, "80-nJ Multipass-Cavity Chirped-Pulse  $\text{Cr}^{4+}$ :forsterite Laser," in *Advanced Solid-State Photonics, OSA Technical Digest Series (CD)* (Optical Society of America, 2010), paper AWE3.

42. Y. Pang, V. Yanovsky, F. Wise, and B. I. Minkov, "Self-mode-locked Cr:forsterite laser," *Opt. Lett.* **18**(14), 1168–1170 (1993).
  43. T.-M. Liu, S.-P. Tai, and C.-K. Sun, "Intracavity frequency-doubled femtosecond  $\text{Cr}^{4+}$ :forsterite laser," *Appl. Opt.* **40**(12), 1957–1960 (2001).
  44. T.-M. Liu, S.-P. Tai, H.-H. Chang, and C.-K. Sun, "Simultaneous multiwavelength generation from a mode-locked all-solid-state Cr:forsterite laser," *Opt. Lett.* **26**(11), 834–836 (2001).
  45. T.-M. Liu, H.-H. Chang, S.-W. Chu, and C.-K. Sun, "Locked multichannel generation and management by use of a Fabry-Perot etalon in a mode-locked Cr:forsterite laser cavity," *IEEE J. Quantum Electron.* **38**(5), 458–463 (2002).
  46. Prime Optical Fiber Corp, "Product information of single-mode optical fiber," [http://www.pofc.com/files/file/financial/SMF130V\\_4.pdf](http://www.pofc.com/files/file/financial/SMF130V_4.pdf).
  47. G. Chang, L.-J. Chen, and F. X. Kärtner, "Highly efficient Cherenkov radiation in photonic crystal fibers for broadband visible wavelength generation," *Opt. Lett.* **35**(14), 2361–2363 (2010).
- 

## 1. Introduction

Emission wavelength is always a critical issue for laser applications. Complementary to Ti:sapphire (0.65 $\mu\text{m}$  – 1.1 $\mu\text{m}$ ) and Cr:YAG lasers (1.4 $\mu\text{m}$  - 1.6 $\mu\text{m}$ ), a Cr:forsterite laser is a desirable femtosecond light source since its operating wavelength is located in the spectral regime from 1.1 $\mu\text{m}$  to 1.4 $\mu\text{m}$  [1]. This spectral regime has attracted much attention in many applications. In biomedical imaging, comparing with the commonly-used 800nm or 1047nm lasers, a Cr:forsterite-laser-based system can acquire sectioned images with a deep penetration depth [2,3] and much reduced photo damage [4–7]. These characteristics open many unique applications on optical coherence tomography (OCT) [2,3], multi-photon microscopy [8–10] and *in vivo* optical harmonics virtual biopsy [11–20]. In selective photothermolysis, the intense light in 1210nm lipid-absorptive band could also be useful for lipid-rich tissues such as fat, sebaceous glands, or atherosclerotic plaques [21]. In nonlinear conversion, difference frequency generation of two Cr:forsterite lasers can generate coherent THz waves from 0.3 to 7.5 THz [22] instead of using a complex optical parametric oscillator (OPO) system. In telecommunication and fiber-based system, the optical pulses in this spectral regime will not broaden significantly as they propagate in an optical fiber. This is of particular importance in both telecommunication system [23] and nonlinear light fiber-microscopy [20,24,25]. Combining with a photonic crystal fiber (PCF), intense Cr:forsterite femtosecond pulses can achieve a super-continuum (SC) white light source with a pulse energy of 1.15 $\mu\text{J}$  [26,27] and broadest ever soliton self-frequency shift to 2.2 $\mu\text{m}$  [28], which is a simple widely-tunable source for various ultrafast applications, including large-dynamic-range RF phase shifter [29].

After the first lasing operation of Cr:forsterite in 1988 [30], great strides were made in optimizing and improving its performance [31–45]. A record-high 2.8W in cryogenic operation [31] and 1.1W at 288K [32] were reported in CW generation. Femtosecond operation was also demonstrated and optical pulses as short as 14~25fs were generated by carefully compensating the cavity dispersion [33,34]. For the potential applications without complicated light source maintenance, stable generation and high output power delivered directly from a single cavity is required. Comparing with the leading material in the field of femtosecond lasers, Ti:sapphire, the thermal conductivity, the excited-state absorption, and high temperature sensitivity of the Cr:forsterite crystal hampered the output power of the forsterite laser [35–37]. Nevertheless, without using complex cavity dump [38] or regenerative amplifier scheme [39], a long cavity with high pulse energy (~17 nJ) and a repetition rate of 26.5MHz [40] was previously achieved by employing a telescope. 80nJ, 5.5ps pulses with a 4.9MHz repetition rate were also demonstrated from a multipass-cavity chirped-pulse forsterite laser [41]. However, the thermal nature of the crystal limits the spectral power density, and thus the applications such as high SNR applications, selective photothermolysis, and high sampling-rate biomedical imaging [17]. In this paper, by relieving the thermal loading of the Cr:forsterite laser crystals, we avoid both the instability performance and gain-saturation behavior at high pump power. As much as 2W CW and 1.4W average output power of sub-100fs pulses were thus demonstrated at 267K. Our study indicates the capability of a Cr:forsterite laser cavity to directly produce stable and high

average power femtosecond pulse trains, which will open many biophotonics [2–21,24,25], spectroscopy, and telecommunication [23] applications.

## 2. Laser cavity design and CW performance

The first step in Cr:forsterite laser construction is the pump source selection. A previous work [31] investigated the operation in Cr:forsterite with several different pump wavelengths, and the result suggested that Nd:YAG laser was a great candidate for the near-the-room-temperature operation. Recently, it has been reported that using the ytterbium fiber laser as the pump source could provide a compact size, more stable operation, longer pumping life time, and a more economic price [40]. Thus, instead of using a Nd:YAG laser as the pump, we employed an Yb: fiber pump laser (PLM-20-1064, IPG), which delivered up to 20W of polarized CW output with a near diffraction limited single-mode beam quality.

The laser resonator employed a conventional Z-fold linear cavity. In order to achieve high output performance at high pump power, we used a pump lens with an 155mm focal length and used curve mirrors with an 150mm radius of curvature, which is longer than the previous works [31–37,40,42–45]. It is to reduce the thermal gradient inside the crystal at a high pumping level. The absorption constant of the Cr:forsterite crystal is also found to be critical for high power performance [35]. In this work, we compared the performances of two Brewster-cut Cr:forsterite crystals, whose absorption constants at the 1064nm pumping wavelength are  $1.4\text{cm}^{-1}$  and  $1.1\text{cm}^{-1}$ , with the same cavity configuration. The dimensions of the crystals were  $3\text{mm}\times 3\text{mm}\times 10.4\text{mm}$  and  $3\text{mm}\times 3\text{mm}\times 13.0\text{mm}$  respectively, which resulted in a 76% single pass absorption. In addition, the temperature of the laser crystal was stabilized and cooled to 270K by a thermo-electric (TE) cooler and a chiller. The crystal was also purged by nitrogen gas to prevent moisture condensation.

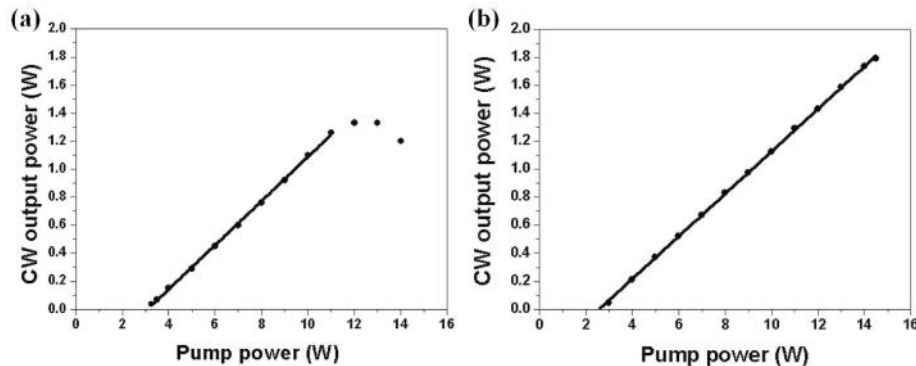


Fig. 1. The output power of the Cr:forsterite laser versus pump power with (a) an  $1.4\text{cm}^{-1}$  absorption constant and (b) an  $1.1\text{cm}^{-1}$  absorption constant: the dots are the experimental data, and the solid lines are the linear fittings. 76% of the incident pump power was absorbed by the crystal.

We first used the crystal with a  $1.4\text{cm}^{-1}$  absorption constant. As shown in Fig. 1(a), the measured CW output power with a 10% output coupler (OC) showed a 15.7% slope efficiency. Above 11W pumping power, the gain-saturation behavior was observed and the output power became unstable even though we adjusted all the components to compensate the thermal-lensing effect. The output power limitation was related to the properties of the crystals, especially the poor thermal conductivity and high temperature sensitivity of the fluorescence lifetime. When high power pumping was applied, the poor thermal conductivity resulted in the severe thermal lensing effect and high equilibrium temperature inside the crystal [35]. The increase of the temperature in forsterite crystals decreases the fluorescence lifetime, and further leads to the decrease of the output power. To overcome the saturation and to relief the thermal stress, we thus compared the performance of using the crystal with a lower absorption constant,  $1.1\text{cm}^{-1}$ . In this scheme, the CW output power could reach 1.8W

under 14.5W pump power with the same 10% OC. As shown in Fig. 1(b), the gain saturation behavior was not observed and the slope efficiency was linear even with a pump level as high as 14.5W. By further cooling the crystal to 267K and by using a 12% OC, CW output power as high as 2W was achieved, with a cavity length of 1.75m.

### 3. Self-starting modelocking operation

To achieve modelocking operation, the positive dispersion in the cavity was compensated by a pair of SF14 prisms with a 31cm tip-to-tip separation and the total cavity length was 1.77m. After finding the stability edge for stable Kerr-lens-modelocking with the 12% OC at a crystal temperature of 267K, stable modelocking operation can be achieved with a 1.4W average output power and an 85MHz repetition rate, under 14.3W pumping power. The performance was characterized via a spectrometer and a home-made autocorrelator. In Fig. 2(a), the modelocked spectrum showed a full width at half maximum (FWHM) of 35nm at a center wavelength of 1251nm. The measured FWHM pulse width was 84 fs by assuming a Gaussian pulse shape. By slightly reducing the pump power to 14.2W, even more stable operation was achieved with an average output power of 1.3W. As shown in Fig. 2(b), the output FWHM spectrum width and a measured FWHM pulse width were 57 nm and 55 fs, respectively. An autocorrelator and a nanosecond-scale response time photodetector were used to check the pulse operation in the fs/ps and nanosecond time scales. No signs of double-pulsing or Q-switch mode-locking were observed. With a time-bandwidth product of 0.59, the output pulse is with a potential to be compressed to 40fs by using external prisms. Without the need of a semiconductor saturable absorber mirror (SESAM) and other starters, this regime was found to be routinely stable without interruption. When the pump was restarted, the femtosecond generation was self-started or it could be easily obtained by prism-shaking. The average power of the laser was recorded after the pump was started and all the alignments were stabilized, and just before the pump was turned off. The fluctuation of the recorded average power was within 5% in a period of two months.

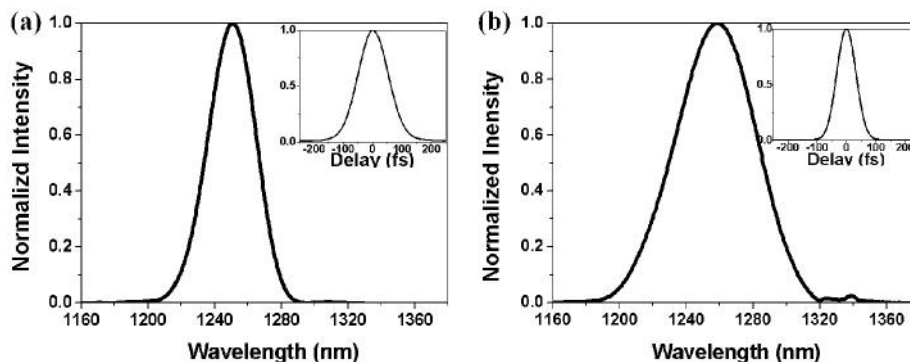


Fig. 2. The spectra and the corresponding autocorrelation traces (inset) of the Cr:forsterite laser with (a) 1.4W and (b) 1.3W output power.

### 4. Fiber-format Cr:forsterite-based light sources

The zero dispersion wavelength of bulk silica is near 1.3 $\mu$ m. As a result, for nonlinear light conversion in fiber using femtosecond Ti:sapphire lasers and Yb: fiber lasers as pump sources, which work in the 0.8 $\mu$ m and 1.0 $\mu$ m wavelength regimes respectively, one has to introduce strong waveguide dispersion for negative fiber dispersion. On the other hand, using a femtosecond Cr:forsterite laser near 1.25 $\mu$ m as the pump source can make the nonlinear light conversion in fiber much easier due to lower requirement on waveguide dispersion. With less need on waveguide dispersion, the corresponding fiber mode-area can be larger and fibers can thus support pulse propagation with higher pulse energy [26–28]. With a 1.3W femtosecond output centered at 1.25 $\mu$ m, the demonstrated laser oscillator could be ideal to support varieties of high power fiber-format light sources.

One example is that additional spectral broadening in fiber pumped by the demonstrated intense Cr:forsterite laser could provide a high spectral density light source covering the 1.0 $\mu\text{m}$  to 1.6 $\mu\text{m}$  wavelength regime. This could be easily achieved with a standard telecommunication single-mode fiber (SMF-130V, POFC) with a core diameter of 9 $\mu\text{m}$ , without the need of a PCF. The fiber nonlinearity  $\gamma = 2\pi n_2(\lambda S)^{-1}$  (here,  $n_2$  is the nonlinear refractive index of the fiber material,  $\lambda$  is the radiation wavelength, and  $S$  is the effective mode area) is about 1.6 $\text{km}^{-1} \text{W}^{-1}$  at  $\lambda = 1.25\mu\text{m}$ . The dispersion length  $L_D = (\Delta T)^2 / |\beta_2|$  (here,  $\Delta T$  is the pulse width and  $\beta_2$  is the second-order dispersion coefficient) is about 1.2m. The fiber bending loss of 100 turns around a mandrel of 60 mm diameter at 1550nm is as small as 0.1dB [46]. With a fiber length of 0.07m to 3.6m and an incident power of 1.1W, Fig. 3 shows the measured SC spectra, covering 1.0 $\mu\text{m}$  to 1.6 $\mu\text{m}$  with a high average output power of 700mW. By shortening the fiber length to 7cm, the temporal distortion in fiber can also be reasonably reduced even without external or pre-compensation. The 7cm-fiber-broadened SC white light source was with an autocorrelation width of 228fs and a 3dB bandwidth of 160nm right after the fiber, as shown in Fig. 3. The fluctuation of the ambient temperature in the laboratory was smaller than 1 $^\circ\text{C}$  and the minimum bending radius was larger than 30mm. The generated SC spectra thus remained stable during the whole measurement period. The negligible fiber bending loss and the stable laser operation could benefit the use for high SNR spectroscopic and biomedical applications.

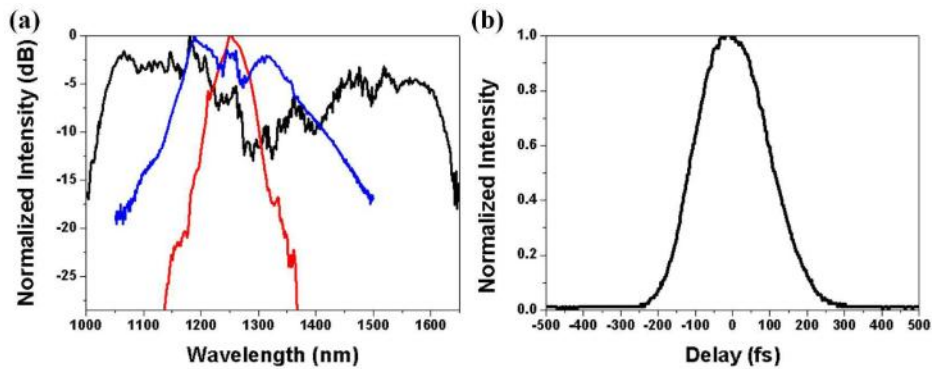


Fig. 3. (a) The spectra of the laser output (red), the fiber output with a fiber length of 3.6m (blue), and the fiber source with a fiber length of 7cm (black). (b) The corresponding autocorrelation trace of the blue spectrum in (a).

Another example of the fiber-format Cr:forsterite-based light sources is the generation of frequency-shifted solitons and the non-radioactive visible light. Our study indicated that the demonstrated intense Cr:forsterite laser could also efficiently suppress the SC generation in selected fibers and provide high power widely-tunable fiber sources by soliton self-frequency shift (SSFS) [28] and the soliton-mediated Cherenkov radiation (CR) [47]. Using a highly nonlinear PCF (SC-5.0-1040, Crystal Fibre A/S) with a zero-dispersion wavelength of 1040nm and a core diameter of 5 $\mu\text{m}$ , octave-spanning widely-tunable fiber sources with high pulse energy could be thus achieved. The fiber nonlinearity  $\gamma$  of the fiber is about 9.1 $\text{km}^{-1} \text{W}^{-1}$  at  $\lambda = 1.25\mu\text{m}$  and the dispersion length  $L_D$  is about 12cm. Figure 4 shows the power dependent spectra of the widely tunable sources, including the simultaneously obtained SSFS in Fig. 4(a) and CR below the wavelength of 1100nm in Fig. 4(b). The threshold of SSFS was  $\sim 20\text{mW}$  and visible CR could be observed above  $\sim 80\text{mW}$  of the total fiber output power. The fiber output spectra could span a range from 550nm to 2273nm with a fiber output power of 340mW, which reached both the upper and lower wavelength-tuning-limit of 2000nm and 550nm due to absorption in this specific fiber. When the fiber output power was 340mW, the average power of the 2000nm soliton was approximately 130mW, corresponding to 1.53nJ pulse energy. As high as 135mW of the broadband CR was also simultaneously obtained.

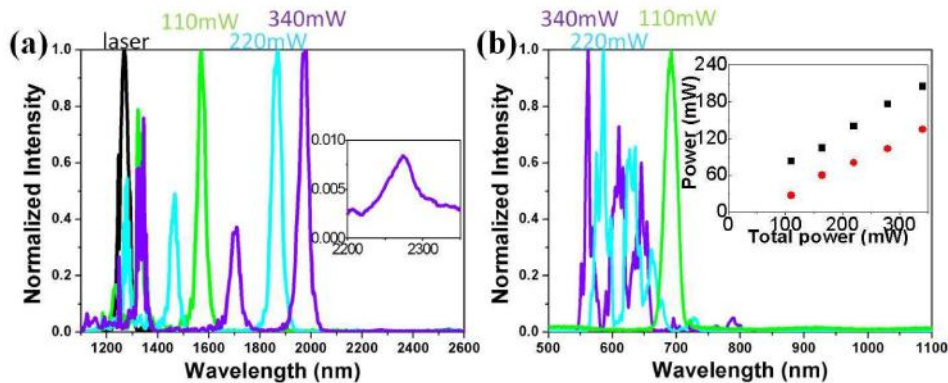


Fig. 4. The power dependent spectra of the widely-tunable fiber-delivered Cr:forsterite source, including the simultaneously obtained SSFS in (a) and CR below the wavelength of 1100nm in (b). The values inserted in the figure represent the total average output power after the photonic crystal fiber. The inset figure in (a) shows the magnified spectra of the 340mW total fiber output ranging from 2200nm to 2350nm. The inset figure in (b) shows the output powers of CR whose wavelength were below 1100nm (red), and the fiber output above the wavelength of 1100nm (black).

## 5. Summary

In this paper, we successfully relieved the thermal loading of the forsterite crystal under 14.5W high pumping power, and have thus demonstrated a Cr:forsterite laser with a high average output power at 267K: 2W in CW and 1.4W under modelocked operation. The demonstration is with twice the average power of the previous work [42] under modelocked operation and is with a shorter pulsewidth. Sub-100fs optical pulse trains with an 85MHz repetition rate and with an >1W average power are achieved from a single Cr:forsterite resonator. Combined with a standard single-mode fiber and a highly nonlinear PCF, broadband SC white light sources with a high spectral density and high peak power, as well as two-octave-spanning widely-tunable sources were also demonstrated, respectively. This demonstrated intense Cr:forsterite laser could thus be potentially applied in many research fields, including high SNR spectroscopic, biomedicine, and microscopic applications.

## Acknowledgement

This project is sponsored by the National Health Research Institute of Taiwan under NHRI-EX99-9936EI, the National Science Council of Taiwan under grant numbers of NSC 96-2628-E-002-043-MY3, and by the National Taiwan University Research Center for Medical Excellence.